Separation of nonstationary sound fields in the time-wavenumber domain

Xiao-Zheng Zhang
Institute of Sound and Vibration Research, Hefei University of Technology, Hefei 230009, People's Republic of China

Jean-Hugh Thomas
Laboratoire d'Acoustique de l'Université du Maine (LAUM UMR-CNRS 6613) and Ecole Nationale Supérieure d'Ingénieurs du Mans, rue Aristote, 72085 Le Mans Cedex 09, France

Chuan-Xing Bi[a)]
Institute of Sound and Vibration Research, Hefei University of Technology, Hefei 230009, People's Republic of China

Jean-Claude Pascal
Laboratoire d'Acoustique de l'Université du Maine (LAUM UMR-CNRS 6613) and Ecole Nationale Supérieure d'Ingénieurs du Mans, rue Aristote, 72085 Le Mans Cedex 09, France

(Received 2 August 2011; revised 10 January 2012; accepted 15 January 2012)

A number of sound field separation techniques have been proposed for different purposes. However, these techniques just consider the separation of sound fields in the space domain and are restricted to stationary sound fields. When the sound fields are nonstationary, it is also necessary to perform the separation in the time domain. Therefore, on the basis of the propagation principle of sound pressure in the time-wavenumber domain, a nonstationary sound field separation technique with two closely spaced parallel measurement surfaces is proposed. It can separate the nonstationary signals generated by the primary sources in both time and space domains when the disturbing sources exist on the other side of the measurement plane. The signals in time and space domains are separated by using the spatial Fourier transform method and the time domain deconvolution method. A simulation involving two monopoles driven by nonstationary signals demonstrates that the method proposed can remove the influence of disturbing sources in both time and space domains. The feasibility of this method is also demonstrated by an experiment with two loudspeakers located on two sides of measurement planes. Additionally, to comment more objectively on the separation results, some indicators are computed in both the simulation and experiment.
 [DOI: 10.1121/1.3683249]

Key Words: 43.60.Sx, 43.60.Pt, 43.60.Gk [EJS] Pages: 2180–2189

I. INTRODUCTION

A number of sound field separation techniques have been proposed for different purposes. The sound field separation technique based on the spatial Fourier transform (SFT) was formally proposed by Tamura[1] to separate the incident and reflected plane-wave components on the surface of the test material, and this separation led to the determination of reflection coefficients at arbitrary angles of incidence. Later, some experimental verifications of this method were also given.[2,3] Cheng *et al.*[4,5] developed this technique to separate the incident and scattered field in both Cartesian and cylindrical coordinate systems and investigated the sensitivity of implementing this separation technique to the measurement parameters and their errors. Yu[6] applied this separation technique to remove the noise sources, overcoming the limitation on applications of nearfield acoustic holography (NAH).[7,8]

The sound field separation technique based on spherical wave expansion was first proposed by Pachner[9] to determine the traveling and standing components of an arbitrary scalar wave field from the measured instantaneous values of the field on the surface of two spheres surrounding the emitter. Weinreich and Arnold[10] used this technique to separate the outgoing waves from the source and incoming waves from reflections by carrying out the measurement on two concentric spheres. Zhao and Wu[11] combined this separation technique with hybrid NAH to reconstruct the vibroacoustic fields in half space.

Both the methods based on SFT and on spherical wave expansion employed double layer pressure measurements. Jacobsen and Jaud[12] proposed a single layer technique on the basis of statistically optimized NAH to separate the primary source form the disturbing source. This method measured both the sound pressure and the normal components of the particle velocity in one measurement plane. Zhang *et al.*[13] modified this method to make the location of the disturbing source arbitrary rather than symmetrical on the side of the measurement plane opposite to that of the primary source.

The preceding sound field separation techniques limited the measurement surface to be regular, such as planar, cylinder, or spherical. Langrenne *et al.*[14] proposed a separation

[a)]Author to whom correspondence should be addressed. Electronic mail: cxbi@hfut.edu.cn

technique based on the boundary element method to recover free field conditions from noisy bounded space situations. Recently Bi *et al.*[15] proposed a sound field separation technique based on equivalent source method to make NAH applications in a field where there exist sources on the two sides of the hologram surface in a reverberant field or in a scattered field. In these two methods, the measurement surface can be arbitrarily shaped.

However, all the above-mentioned techniques were only used with stationary sound fields, and the separations were just applied in the space domain. In the presence of nonstationary sound fields, for separating the time-dependent incident and reflected wave components to determine the reflection coefficients on the surface of test materials over a wide frequency range in a single measurement or for separating the time-dependent incident and scattered fields when the scattering bodies exist in the sound field or for removing the disturbance from noise sources when applying time domain holography[16] or real-time nearfield acoustic holography[17,18] to study the sound radiation in confined industrial places, all the separations should be done in both time and space domains. Until now, it seems that no research has been done considering the separation technique in both time and space domains for nonstationary sound fields. In this paper, a nonstationary sound field separation technique is proposed based on the propagation principle of sound pressure in the time-wavenumber domain. The approach leading to the reconstruction of the pressure field radiated by the primary source is described in Sec. II. To investigate the performance of the method proposed in both time and space domains, a simulation study with two monopole sources is carried out and reported in Sec. III. Section IV presents an experiment with two loudspeakers located on the two sides of measurement planes to demonstrate the feasibility of the method proposed.

II. NONSTATIONARY SOUND FIELD SEPARATION TECHNIQUE

The technique is based on the use of two measurement planes close to each other. The configuration is shown in Fig. 1, where source 1 is the primary source, source 2 is the disturbing source, and the distance between measurement plane 1 and measurement plane 2 is $\Delta z = z_2 - z_1$. Each measurement plane provides the contribution of the primary source and also the contribution of the disturbing source. The aim of the separation technique is to remove the contribution of the disturbing source on measurement plane 1. For this purpose, the contribution of the disturbing source on measurement plane 1 is predicted by using the pressure field acquired from measurement plane 2, which is propagated to measurement plane 1. Then the predicted disturbing acoustic field is subtracted from the acoustic field recorded on measurement plane 1, yielding a formulation of the pressure field acquired from measurement plane 1 and due to the primary source alone.

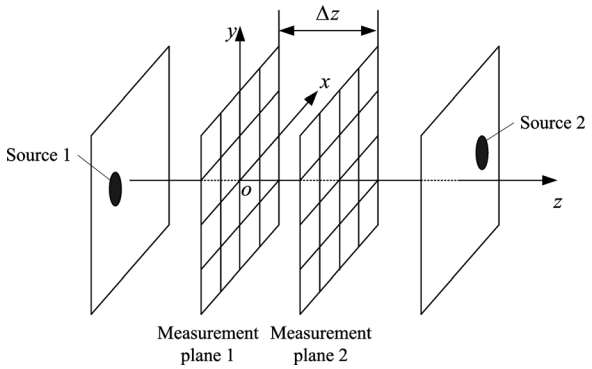

FIG. 1. Configuration of the separation system. Source 1 is the primary source, source 2 is the disturbing source and the distance between measurement plane 1 and measurement plane 2 is $\Delta z = z_2 - z_1$.

In the following, the steps of the separation technique are described. The sound pressure $p(x,\ y,\ z_1,\ t)$ acquired from measurement plane 1 equals the sum of the sound pressure $p_1(x,\ y,\ z_1,\ t)$ generated by source 1 and the sound pressure $p_2(x,\ y,\ z_1,\ t)$ generated by source 2, that is

$$p(x,\ y,\ z_1,\ t) = p_1(x,\ y,\ z_1,\ t) + p_2(x,\ y,\ z_1,\ t). \tag{1}$$

By applying the two-dimensional Fourier transform with respect to x and y to Eq. (1), and using the time-wavenumber spectrum $P(k_x,\ k_y,\ z,\ t)$ given by

$$P(k_x,\ k_y,\ z,\ t) = \int_{-\infty}^{\infty}\int_{-\infty}^{\infty} p(x,y,\ z,\ t)e^{j(k_x x + k_y y)}dxdy, \tag{2}$$

Eq. (1) yields

$$P(k_x,\ k_y,\ z_1,\ t) = P_1(k_x,\ k_y,\ z_1,\ t) + P_2(k_x,\ k_y,\ z_1,\ t). \tag{3}$$

Similarly, the time-wavenumber spectrum $P(k_x,\ k_y,\ z_2,\ t)$ on measurement plane 2 equals the sum of the time-wavenumber spectrum $P_1(k_x,\ k_y,\ z_2,\ t)$ generated by source 1 and the time-wavenumber spectrum $P_2(k_x,\ k_y,\ z_2,\ t)$ generated by source 2, that is

$$P(k_x,\ k_y,\ z_2,\ t) = P_1(k_x,\ k_y,\ z_2,\ t) + P_2(k_x,\ k_y,\ z_2,\ t). \tag{4}$$

According to the forward propagation formulation of the sound pressure in the time-wavenumber domain as shown in Ref. 19, the relationships between the time-wavenumber spectra of pressures radiated from a single source on both planes can be written as

$$P_1(k_x,\ k_y,\ z_2,\ t) = P_1(k_x,\ k_y,\ z_1,\ t) * h(k_x,\ k_y,\ \Delta z,\ t), \tag{5}$$

$$P_2(k_x,\ k_y,\ z_1,\ t) = P_2(k_x,\ k_y,\ z_2,\ t) * h(k_x,\ k_y,\ \Delta z,\ t), \tag{6}$$

where $h(k_x,\ k_y,\ \Delta z,\ t)$ is the impulse response function that is given by

$$h(k_x,k_y,\Delta z,t)=\delta(t-\Delta z/c)-\Delta z\sqrt{k_x^2+k_y^2}\times\frac{J_1\left(c\sqrt{k_x^2+k_y^2}\sqrt{t^2-\Delta z^2/c^2}\right)}{\sqrt{t^2-\Delta z^2/c^2}}\times H(t-\Delta z/c),\tag{7}$$

where c denotes the sound velocity, $\delta(t)$ denotes the Dirac delta function, J_1 denotes the Bessel function of the first kind and order 1, and $H(t)$ denotes the Heaviside function.

Substituting Eq. (5) into Eq. (4) leads to

$$P(k_x,\ k_y,\ z_2,\ t)=P_1(k_x,\ k_y,\ z_1,\ t)*h(k_x,\ k_y,\ \Delta z,\ t)+P_2(k_x,\ k_y,\ z_2,\ t).\tag{8}$$

Similarly, substituting Eq. (6) into Eq. (3) yields

$$P(k_x,\ k_y,\ z_1,\ t)=P_1(k_x,\ k_y,\ z_1,\ t)+P_2(k_x,\ k_y,\ z_2,\ t)*h(k_x,\ k_y,\ \Delta z,\ t).\tag{9}$$

Applying the convolution with the impulse response function $h(k_x,\ k_y,\Delta z,\ t)$ to both sides of Eq. (8) and then subtracting from Eq. (9) gives

$$\begin{aligned}&P(k_x,\ k_y,\ z_1,\ t)-P(k_x,\ k_y,\ z_2,\ t)*h(k_x,\ k_y,\ \Delta z,\ t)\\&=P_1(k_x,\ k_y,\ z_1,\ t)-P_1(k_x,\ k_y,\ z_1,\ t)*h(k_x,\ k_y,\ \Delta z,\ t)*h(k_x,\ k_y,\ \Delta z,\ t)\\&=P_1(k_x,\ k_y,\ z_1,\ t)*[\delta(t)-h(k_x,\ k_y,\ \Delta z,\ t)*h(k_x,\ k_y,\ \Delta z,\ t)].\end{aligned}\tag{10}$$

The left part of Eq. (10) is obtained by applying the spatial two-dimensional Fourier transform to the spatial pressure fields acquired from both measurement planes, yielding $P(k_x,\ k_y,\ z_1,\ t)$ and $P(k_x,\ k_y,\ z_2,\ t)$ and by using $h(k_x,\ k_y,\ \Delta z,\ t)$, which is known. Six methods for calculating the impulse response were presented in Ref. 19. Grulier *et al*. showed that the inverse Fourier transform method and the numerical Kaiser method provided the most accurate results among the six methods tested. As the numerical Kaiser method is much more time-consuming than the inverse Fourier transform method, the inverse Fourier transform method is used here. Finally, the time-wavenumber spectrum $P_1(k_x,\ k_y,\ z_1,\ t)$ on measurement plane 1 generated by the primary source can be solved by operating the deconvolution of Eq. (10).

By setting

$$A(k_x,\ k_y,\ t)=P(k_x,\ k_y,\ z_1,\ t)-P(k_x,\ k_y,\ z_2,\ t)*h(k_x,\ k_y,\ \Delta z,\ t),\tag{11}$$

$$B(k_x,\ k_y,\ t)=\delta(t)-h(k_x,\ k_y,\ \Delta z,\ t)*h(k_x,\ k_y,\ \Delta z,\ t),\tag{12}$$

Eq. (10) can be rewritten as

$$A(k_x,\ k_y,\ t)=P_1(k_x,\ k_y,\ z_1,\ t)*B(k_x,\ k_y,\ t).\tag{13}$$

Equation (13) acts in the continuous time domain. To implement Eq. (13), the time variable t should be discretized as t_1, t_2, …, t_N. Then, according to the discrete convolution formula, Eq. (13) can be discretized as

$$A(k_x,\ k_y,\ t_n)=\sum_{i=1}^{n}P_1(k_x,\ k_y,\ z_1,\ t_i)B(k_x,\ k_y,\ t_{n+1-i}),\quad n=1,\ldots,N.\tag{14}$$

For each $(k_x,\ k_y)$ in the wavenumber domain, Eq. (14) can be written in a matrix form as

$$\mathbf{A}=\mathbf{B}\mathbf{P}_1,\tag{15}$$

where

$$\mathbf{A}=[A(k_x,\ k_y,t_1)\quad A(k_x,\ k_y,t_2)\quad\cdots\quad A(k_x,\ k_y,t_N)]^T,\tag{16}$$

$$\mathbf{P}_1=[P_1(k_x,\ k_y,\ z_1,\ t_1)\quad P_1(k_x,\ k_y,\ z_1,\ t_2)\cdots P_1(k_x,\ k_y,\ z_1,\ t_N)]^T,\tag{17}$$

$$\mathbf{B}=\begin{bmatrix}B(k_x,\ k_y,t_1) & 0 & \cdots & 0\\ B(k_x,\ k_y,t_2) & B(k_x,\ k_y,t_1) & \ddots & \vdots\\ \vdots & \ddots & \ddots & 0\\ B(k_x,\ k_y,t_N) & \cdots & B(k_x,\ k_y,t_2) & B(k_x,\ k_y,t_1)\end{bmatrix}.\tag{18}$$

In Eq. (15), both $\mathbf{A}$ and $\mathbf{B}$ are known, and $\mathbf{P}_1$ is to be calculated. In practice, because the data in A are always contaminated by some errors, such as the measurement error and the calculation error of the impulse response, coupled with the ill-posed process of solving $\mathbf{P}_1$, these errors will lead to an inappropriate solution in the inversion process. To obtain an appropriate solution, the singular value decomposition (SVD) and the standard Tikhonov regularization[20] are used.

Define the SVD of the matrix $\mathbf{B}$ as

$$\mathbf{B} = \mathbf{U}\mathbf{S}\mathbf{V}^H, \tag{19}$$

where $\mathbf{U}$ and $\mathbf{V}$ are the left and right unitary (orthonormal) matrices, respectively, $\mathbf{V}^H$ is the conjugate transpose of $\mathbf{V}$, and $\mathbf{S}$ is the diagonal matrix of singular values. By substituting Eq. (19) into Eq. (15) and solving the inverse of $\mathbf{B}$, the non-regularized solution of Eq. (15) is obtained by

$$\mathbf{P}_1 = \mathbf{V}\mathbf{S}^{-1}\mathbf{U}^H\mathbf{A} = \sum_{n=1}^{N} \frac{\mathbf{u}_n^H\mathbf{A}}{s_n}\mathbf{v}_n, \tag{20}$$

where s_n is the nth singular value of $\mathbf{B}$. The regularization acts as a filter on the singular values of $\mathbf{B}$, yielding the regularized solution

$$\mathbf{P}_1^{\lambda} = \sum_{n=1}^{N} f_n \frac{\mathbf{u}_n^H\mathbf{A}}{s_n}\mathbf{v}_n, \tag{21}$$

where f_n are the coefficients of the regularization filter. In the case of standard Tikhonov regularization, the filter coefficients f_n are given by

$$f_n = \frac{s_n^2}{s_n^2 + \lambda^2}, \tag{22}$$

where λ is the regularization parameter, selected by the L-curve method.[21]

Once the regularized solution $\mathbf{P}_1^{\lambda}$ is obtained for each wavenumber (k_x, k_y) by Eq. (21), the sound pressure $p_1(x, y, z_1, t)$ on measurement plane 1, generated by the primary source, can be separated in both time and space domains by applying the inverse Fourier transform with respect to k_x and k_y to $\mathbf{P}_1^{\lambda}$.

III. NUMERICAL SIMULATION

To investigate the performance of the method proposed, a simulation study with two monopole sources is carried out. The geometric description of sources and measurement planes is shown in Fig. 2. Source 1 located at (0.252 m, 0.324 m, −0.15 m) is considered as the primary source that generates a nonstationary signal with a linear frequency modulation in the [200, 1800] Hz band and a Gaussian amplitude modulation. Source 2 located at (0.432 m, 0.324 m, 0.18 m) is considered as the disturbing source that also generates a nonstationary signal – Morlet wavelet defined by

$$s(t) = \cos(2\pi f_0 t)e^{-t^2/2}, \tag{23}$$

where $f_0 = 800$ Hz. Each measurement plane provides 19×19 measurement points. In this simulation, the theoretical sound pressure at each measurement point is calculated by using the following equation

$$p(R, t) = \frac{s(t - R/c)}{4\pi R}, \tag{24}$$

where $s(t)$ denotes the input signal, and R denotes the distance between the measurement point and the monopole source. Considering that the Nyquist sampling rate requires the spacing of measurement points to be less than half the shortest wavelength of the signal generated by the primary source ($\lambda_{\min}$ corresponds to the maximum frequency 1800 Hz), the spacing of measurement points in both x and y directions is set to $a = 0.036$ m $< \lambda_{\min}/2 = 0.096$ m. Then the size of the measurement plane, namely 0.648×0.648 m^2, is large enough to almost cover the whole sound field and to avoid the significant discontinuity at the measurement edge. Measurement plane 1 is located at $z_1 = 0$ m, and measurement plane 2 is located at $z_2 = 0.03$ m. The simulated signals are sampled at a frequency $f_e = 34\,400$ Hz providing 256 samples. Because the pressure signal generated by the disturbing source on measurement plane 1 is to be removed finally, it can be seen as the "noise," while the pressure signal generated by the primary source on measurement plane 1 is seen as the signal of interest. The calculated mean signal-to-noise ratio (SNR) on measurement plane 1 is 3.8 dB. In the separation process, the Tikhonov regularization method is used, and the regularization parameter values selected by the L-curve method for each wavenumber (k_x, k_y) are shown in Fig. 3. Besides, to lessen the wrap-around errors due to the use of discrete two-dimensional spatial Fourier transforms

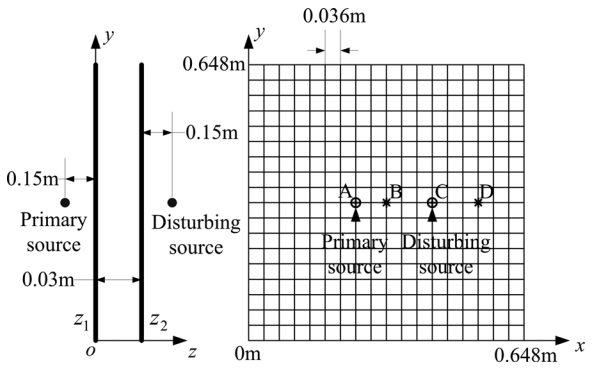

FIG. 2. Geometric description of sources and measurement planes. Points A and C, marked with +, stand for the points facing the primary source and the disturbing source, respectively. Points B and D, marked with *, stand for the points not facing sources.

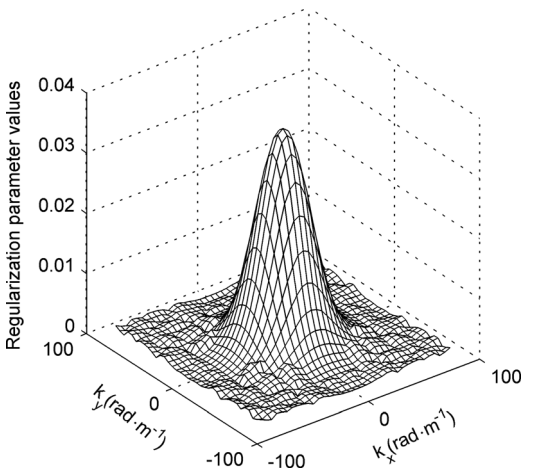

FIG. 3. Regularization parameter values selected by the L-curve method for each wavenumber (k_x, k_y).

associated with the finite size of the hologram, the 19×19 pressure matrices on the measurement planes are extended to 37×37 matrices by zero-padding.[7]

To assess the relevance of the proposed separation technique in the time domain, four space points on measurement plane 1 are selected, and their positions are A (0.252 m, 0.324 m, 0 m), B (0.324 m, 0.324 m, 0 m), C (0.432 m, 0.324 m, 0 m), and D (0.540 m, 0.324 m, 0 m), respectively. As shown in Fig. 2, points A and C are facing the primary source and the disturbing source, respectively, point B is located at the center of measurement plane 1, and point D is close to the edge of measurement plane 1. The theoretical pressure radiated by the primary source (line with circles) and the theoretical pressure radiated by the disturbing source (line with plus signs) at these four points are shown in Fig. 4. Note that the strength ratios of these two pressures are different at four space points; for example, the pressure strength radiated by the primary source is larger than that radiated by the disturbing source at point A but smaller at point D. It is conceivable that this difference will lead to different qualities of separation results. The lines with solid points in Fig. 4 denote the theoretical pressure including the contributions of the primary source and the disturbing source. The comparison results between lines with circles and lines with solid points indicate that the pressure signals radiated by the primary source are contaminated by the "noise" radiated by the disturbing source. To remove the influence of disturbing source and extract the pressure radiated by the primary source, the separation technique proposed is used. The calculated pressures (line with crosses)

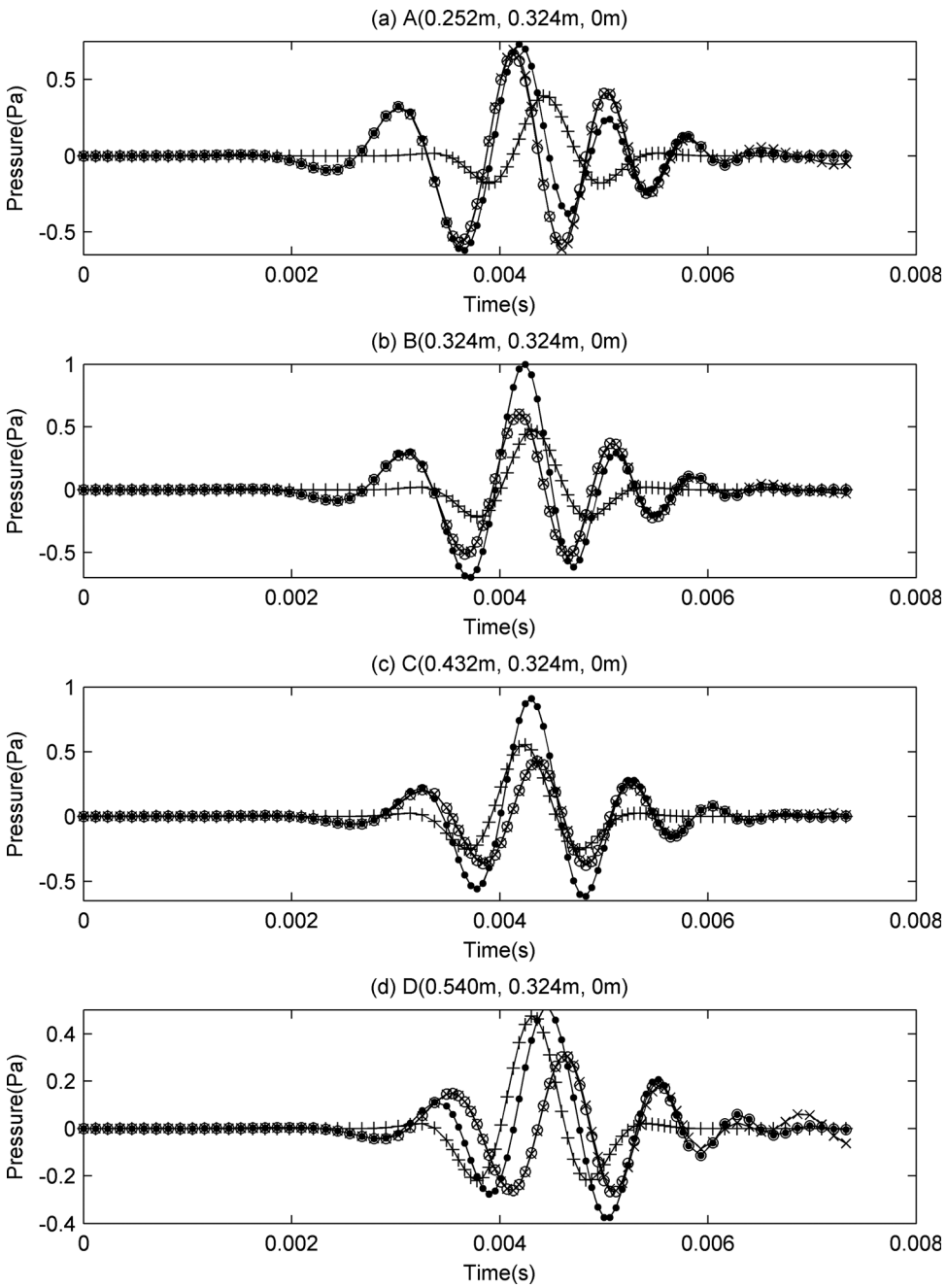

FIG. 4. Comparison between the time pressure signals on measurement plane 1 in points A (a), B (b), C (c), and D (d): The theoretical pressure radiated by the primary source (line with circles), the theoretical pressure radiated by the disturbing source (line with plus signs), the theoretical pressure including the contributions of the primary source and the disturbing source (line with solid points), and the calculated pressure using the separation technique (line with crosses).

are shown in Fig. 4. Obviously, the calculated pressures match well with the theoretical pressures radiated by the primary source at four points except that some slight residual distortions appear at the ends of the separated pressure signals. In conclusion, the separation results demonstrate that the method proposed can remove or highly reduce the radiation contribution due to the disturbing source.

To comment more objectively on the separation results in the time domain, two time indicators T_1 and T_2 are calculated for a point (x_i, y_j) on measurement plane 1. They are defined by

$$T_1(x_i,y_j)=\frac{\langle p_a(x_i,y_j,z_1,t)p_c(x_i,y_j,z_1,t)\rangle_t}{\sqrt{\langle p_a^2(x_i,y_j,z_1,t)\rangle_t\langle p_c^2(x_i,y_j,z_1,t)\rangle_t}}, \tag{25}$$

$$T_2(x_i,y_j)=\frac{\left|p_a^{rms}(x_i,y_j,z_1)-p_c^{rms}(x_i,y_j,z_1)\right|}{p_a^{rms}(x_i,y_j,z_1)}, \tag{26}$$

where $p_a^{rms}(x_i,y_j,z_1)$ and $p_c^{rms}(x_i,y_j,z_1)$ are the root mean square pressure values given by

$$p_a^{rms}(x_i,y_j,z_1)=\sqrt{\langle p_a^2(x_i,y_j,z_1,t)\rangle_t}, \tag{27}$$

$$p_c^{rms}(x_i,y_j,z_1)=\sqrt{\langle p_c^2(x_i,y_j,z_1,t)\rangle_t}. \tag{28}$$

$\langle\ \rangle_t$ denotes the time averaged value. $p_a(x_i,y_j,z_1,t)$ is the theoretical time-dependent pressure, and $p_c(x_i,y_j,z_1,t)$ is the calculated time-dependent pressure using the separation technique. T_1 and T_2 are sensitive to the phase difference and magnitude difference between $p_a(x_i,y_j,z_1,t)$ and $p_c(x_i,y_j,z_1,t)$, respectively. Phase accuracy gives T_1 in the neighborhood of 1, and magnitude accuracy gives T_2 near 0. The values of both indicators T_1 and T_2 are computed for each measurement point. The map of indicator T_1 with the 0.99 contour line is shown in Fig. 5(a), and the map of indicator T_2 with the 0.05 contour line is shown in Fig. 5(b). From the indicator values shown in Fig. 5, it can be seen that for most space points in the time domain, the pressure resulting from the separation technique matches very well the theoretical pressure, and a lower accuracy mainly appears near the edge of measurement plane 1. The values of indicator T_1 at marked points A(+), B(*), C(+), and D(*) are 0.997, 0.999, 0.999, and 0.986, respectively. The values of indicator T_2 at marked points A(+), B(*), C(+), and D(*) are 0.028, 0.003, 0.021, and 0.006, respectively.

Similarly, for highlighting the relevance of the proposed separation technique in the space domain, two random time instants ($t_1=4.2$ ms and $t_2=5.0$ ms) are chosen. Figures 6(a), 6(b), and 6(c) show the theoretical pressure p_a radiated by the primary source, the theoretical pressure p_b including the contributions of the primary source and the disturbing source, and the calculated pressure p_c resulting from the separation technique at $t_1=4.2$ ms, respectively. Figures 6(d), 6(e), and 6(f) show the same sound fields but at $t_2=5.0$ ms. Obviously, the proposed separation technique demonstrates its ability to eliminate the disturbance from source 2 in the space domain.

To evaluate the quality of the separation results in the space domain, a spatial error criteria is introduced and defined by

$$E_{x,y}^r(t_n)=\frac{\sqrt{\langle(p_c(x,y,t_n)-p_a(x,y,t_n))^2\rangle_s}}{\sqrt{\langle p_a^2(x,y,t_n)\rangle_s}}, \tag{29}$$

which corresponds to the relative error between the pressure calculated using the separation technique $p_c(x,y,t_n)$ and the theoretical pressure $p_a(x,y,t_n)$ radiated from the primary source at a given time t_n, and $\langle\ \rangle_s$ denotes the spatial averaged value. The time evolution of the relative error is shown in Fig. 7, which illustrates that at most time instants the pressure resulting from the separation technique is close to the theoretical pressure field radiated by the primary source in the space domain. High values of the relative spatial error are obtained at the edges of the signal due to the fact that the theoretical pressure field supplies the denominator of Eq. (29) with very low values at these time instants. The values of the relative error at $t_1=4.2$ ms and $t_2=5.0$ ms are 0.044 and 0.088, respectively.

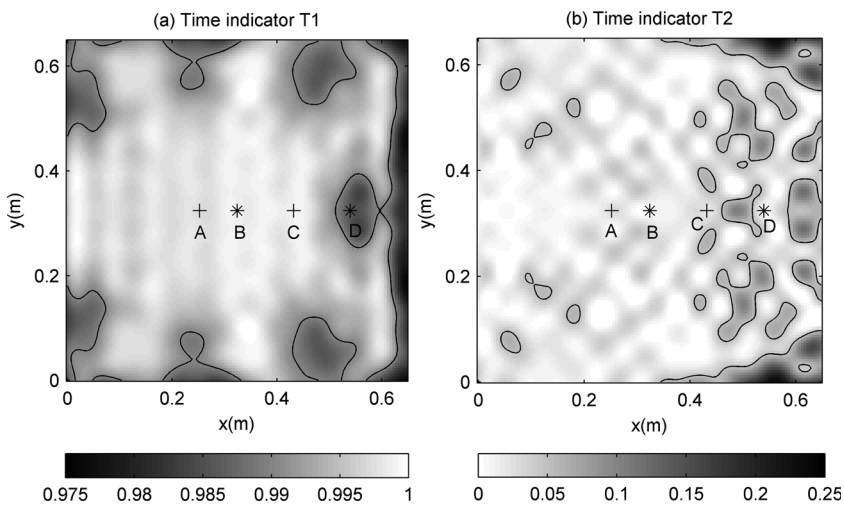

FIG. 5. Spatial maps for the indicator T_1 (a) with a contour line at the value 0.99 and for the indicator T_2 (b) with a contour line at the value 0.05.

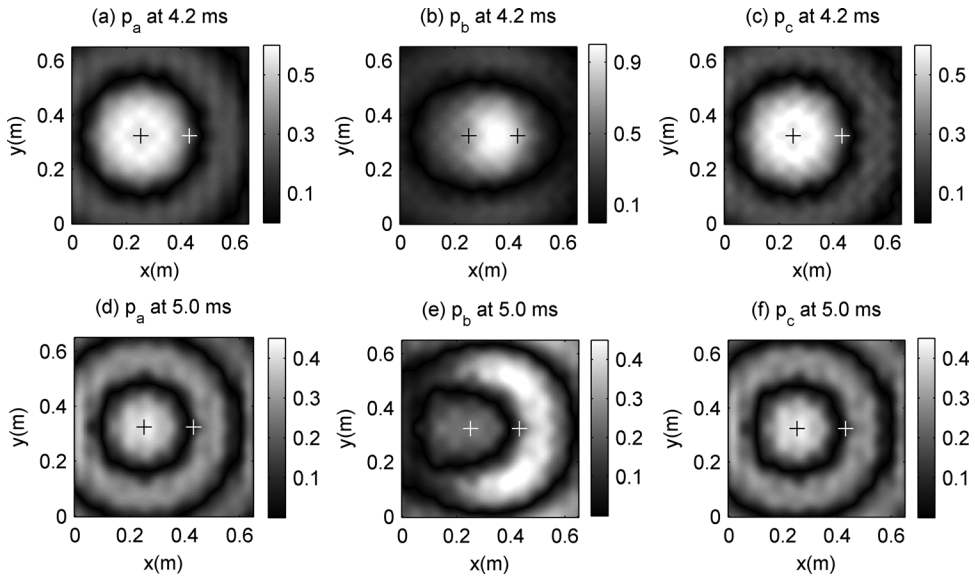

FIG. 6. Simulated results: theoretical spatial pressure field p_a radiated by the primary source at $t_1 = 4.2$ ms (a) and at $t_2 = 5.0$ ms (d), theoretical spatial pressure field p_b including the contributions of the primary source and the disturbing source at $t_1 = 4.2$ ms (b) and at $t_2 = 5.0$ ms (e), and spatial pressure field p_c resulting from the separation technique at $t_1 = 4.2$ ms (c) and at $t_2 = 5.0$ ms (f). The left marked location is facing the primary source and the right marked location is facing the disturbing source.

IV. EXPERIMENT

To examine the feasibility of the proposed sound field separation techniques, an experiment is carried out. The experimental setup is shown in Fig. 8.

Two loudspeakers are selected as the primary source and the disturbing source, respectively. The signals generated by these two sources are very similar to those used in the simulation case. These signals are also recorded at a sampling frequency $f_e = 34\,400$ Hz providing 256 samples.

In addition, the experiment provides the same locations of sources and measurement planes as those in the simulation case. A double-layer microphone array with an interval of 0.03 m, shown in Fig. 8, is used to measure simultaneously the pressure fields on both measurement plane 1 and measurement plane 2. Each layer provides 2×4 microphones equally spaced every 0.036 m. For each measurement the array is moved, both sources are synchronized and generated exactly the same signals to simulate the simultaneous sound field acquisition on a large area composed of 19×19 measurement points providing an overall scan area of 0.648 m $\times$ 0.648 m. The calculated mean SNR on measurement plane 1 is 4.7 dB.

As in the simulation case, the same Tikhonov regularization method and zero-padding method are used in the separation process of experiment. Moreover, an exponential filter[2] with the optimal selected parameters $k_c = 80$ rad/m and $\alpha = 1.0$ is employed in the experiment to further improve the accuracy of separation results.

Four space points, with the same locations as those in the simulation case, are selected to show the results in the time domain from the separation technique. Figure 9 shows the measured pressure radiated by the primary source (line with circles), the measured pressure radiated by the disturbing source (line with plus signs), the measured pressure including the contributions of the primary source and the disturbing source (line with solid points), and the calculated pressure using the separation technique (line with crosses). The comparison results between the lines with circles and the lines with solid points indicate the measurements are affected by the disturbing source in different degrees at four points. The comparison results between the lines with circles and the lines with crosses show that the calculated pressures using the separation technique match well with the measured pressures radiated by the primary source, which demonstrate

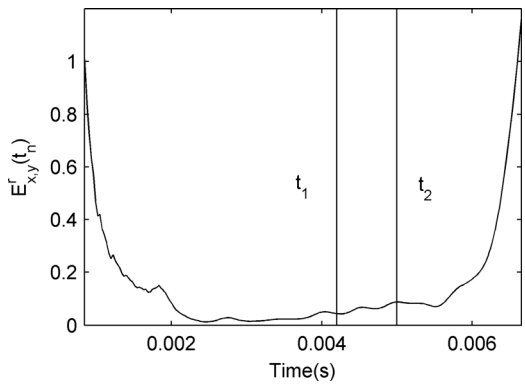

FIG. 7. Time evolution of the relative error $E^r_{x,y}$ between the pressure calculated using the separation technique and the theoretical pressure radiated from the primary source. The vertical lines indicate the chosen time instants $t_1 = 4.2$ ms and $t_2 = 5.0$ ms.

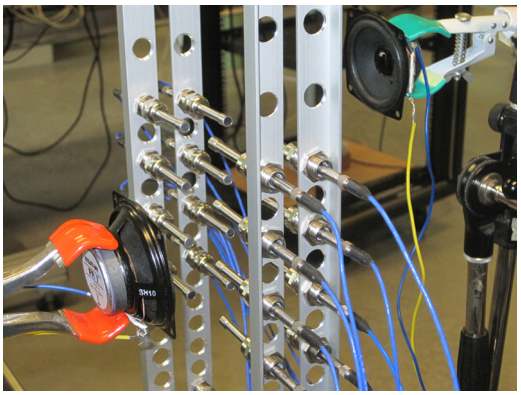

FIG. 8. (Color online) Experimental setup with two loudspeakers and a double-layer microphone array.

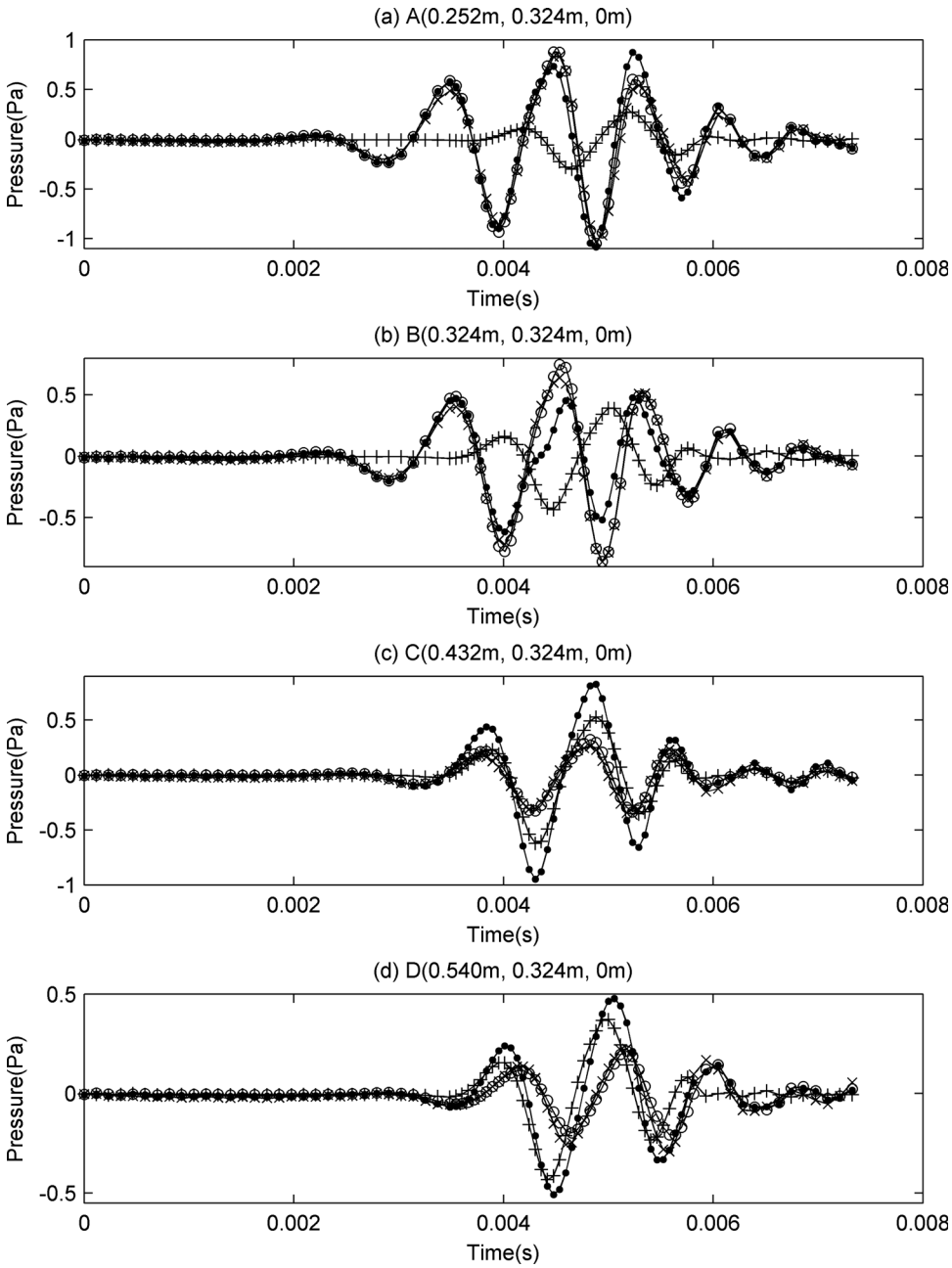

FIG. 9. Comparison between the time pressure signals on measurement plane 1 in points A (a), B (b), C (c), and D (d): The measured pressure radiated by the primary source (line with circles), the measured pressure radiated by the disturbing source (line with plus signs), the measured pressure including the contributions of the primary source and the disturbing source (line with solid points), and the calculated pressure using the separation technique (line with crosses).

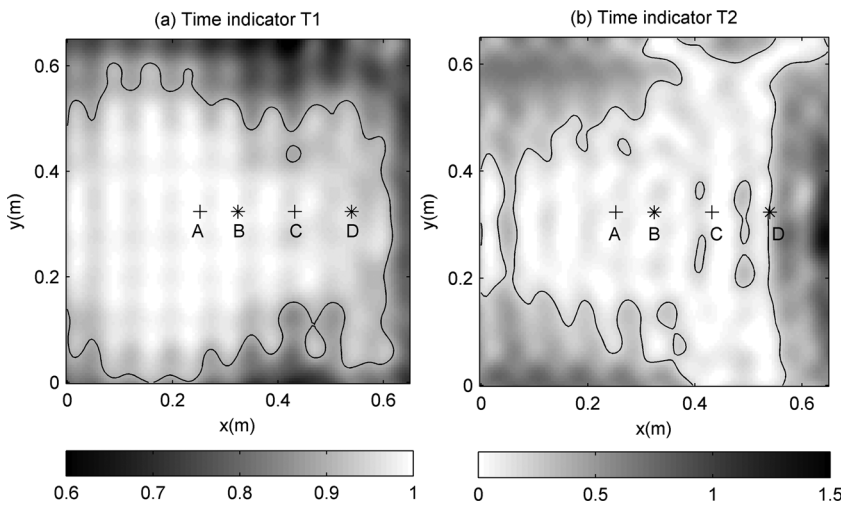

FIG. 10. Spatial maps for the indicator T_1 (a) with a contour line at the value 0.9 and for the indicator T_2 (b) with a contour line at the value 0.2.

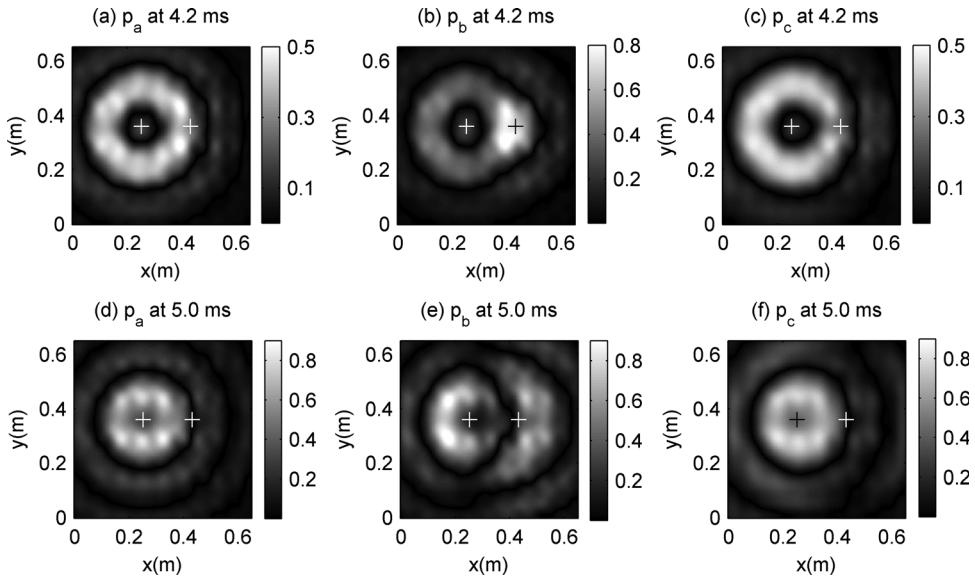

FIG. 11. Experimental results: measured spatial pressure field p_a radiated by the primary source at $t_1 = 4.2$ ms (a) and at $t_2 = 5.0$ ms (d), measured spatial pressure field p_b including the contributions of the primary source and the disturbing source at $t_1 = 4.2$ ms (b) and at $t_2 = 5.0$ ms (e), and spatial pressure field p_c resulting from the separation technique at $t_1 = 4.2$ ms (c) and at $t_2 = 5.0$ ms (f). The left marked location is facing the primary source and the right marked location is facing the disturbing source.

that the separation technique has a good ability of removing the influence of the disturbing source in the time domain.

Indicators T_1 and T_2 are also computed for each location facing the microphone positions from the measured pressure p_a radiated by the primary source and the calculated pressure p_c resulting from the separation technique. The map of indicator T_1 with the 0.9 contour line is shown in Fig. 10(a), and the map of indicator T_2 with the 0.2 contour line is shown in Fig. 10(b). Figure 10 indicates that the separation works well for most space points in the time domain even if the indicator values are less accurate than those from the simulation case. The values of indicator T_1 at marked points A(+), B(*), C(+), and D(*) are 0.993, 0.994, 0.971, and 0.955, respectively. The values of indicator T_2 at marked points A(+), B(*), C(+), and D(*) are 0.061, 0.058, 0.003, and 0.230, respectively.

The separation results in the space domain are studied for the two time instants selected in the simulation case ($t_1 = 4.2$ ms and $t_2 = 5.0$ ms). Figures 11(a), 11(b), and 11(c) show the measured pressure p_a radiated by the primary source, the measured pressure p_b including the contributions of the primary source and the disturbing source, and the calculated pressure p_c resulting from the separation technique at $t_1 = 4.2$ ms, respectively. Figures 11(d), 11(e), and 11(f) show the same sound fields but at $t_2 = 5.0$ ms. Obviously, the proposed separation technique seems effective to suppress the sound radiated by the disturbing source in the space domain.

The relative spatial error defined in Eq. (29) is calculated for each time t_n. Its time evolution is shown in Fig. 12, which highlights a similar trend as that in Fig. 7 but with less accurate values. The values of the relative error at $t_1 = 4.2$ ms and $t_2 = 5.0$ ms are 0.247 and 0.305, respectively.

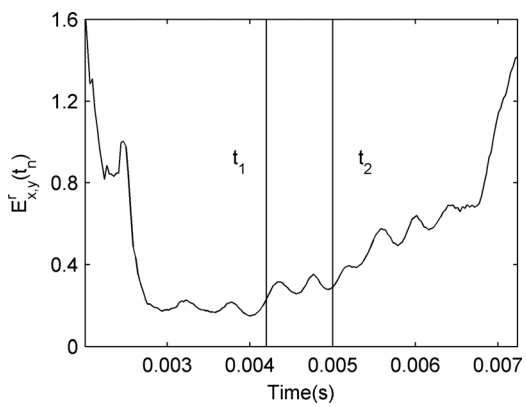

FIG. 12. Time evolution of the relative error $E^r_{x,y}$ between the pressure calculated using the separation technique and the measured pressure radiated from the primary source. The vertical lines indicate the chosen time instants $t_1 = 4.2$ ms and $t_2 = 5.0$ ms.

V. CONCLUSIONS

The existing sound field separation techniques can only be used in the presence of stationary sound fields. In this paper, a nonstationary sound field separation technique is proposed. The method performs the separation in both time and space domains. In the time domain, the signals generated by the primary source are separated using a deconvolution method. A simulation involving two monopoles driven by nonstationary signals demonstrates that the method proposed can well remove the influence of the disturbing source in both time and space domains. The feasibility of the method proposed is also investigated through an experiment with two loudspeakers located on the two sides of measurement planes. To comment more objectively the separation results, some indicators are introduced to both time and space domains. The computed values of these indicators demonstrate the results obtained in the simulation case are satisfactory, while the results obtained in the experimental case are a little worse. Therefore the experiment has to be further improved in the future by enhancing the experimental conditions and investigating some parameters, such as the size of the measurement plane, the distance between two measurement planes, the spacing of measurement points, the SNR, and the source locations, etc.

ACKNOWLEDGMENTS

This work was supported by National Natural Science Foundation of China (Grants No. 10974040 and No. 51105126), the Program for New Century Excellent Talents in University (Grant No. NCET-08-0767), and the Research Fund for the Doctoral Program of Higher Education (Grant No. 20100111110007). The authors would like to thank Julien Nicolas from the Ecole Nationale d'Ingénieurs du Mans (ENSIM) for his contribution to the building of the double-layer array.

[1]M. Tamura, "Spatial Fourier-transform method for measuring reflection coefficients at oblique incidence. I. Theory and numerical examples," J. Acoust. Soc. Am. **88**(5), 2259–2264 (1990).
[2]M. Tamura, J. F. Allard, and D. Lafarge, "Spatial Fourier-transform method for measuring reflection coefficients at oblique incidence. II. Experimental results," J. Acoust. Soc. Am. **97**(4), 2255–2262 (1995).
[3]Z. Hu and J. S. Bolton, "The measurement of plane-wave reflection coefficients by using two-dimensional spatial transforms," J. Acoust. Soc. Am. **88**(S1), S173 (1990).
[4]M. T. Cheng, J. A. Mann III, and A. Pate, "Wave-number domain separation of the incident and scattered sound field in Cartesian and cylindrical coordinates," J. Acoust. Soc. Am. **97**(4), 2293–2303 (1995).
[5]M. T. Cheng, J. A. Mann III, and A. Pate, "Sensitivity of the wave-number domain field separation methods for scattering," J. Acoust. Soc. Am. **99**(6), 3550–3557 (1996).
[6]F. Yu, J. Chen, W. B. Li, and X. Z. Chen, "Sound field separation technique and its applications in near-field acoustic holography," Acta Phys. Sin. **54**(2), 789–797 (2005).
[7]J. D. Maynard, E. G. Williams, and Y. Lee, "Nearfield acoustic holography. I. Theory of generalized holography and development of NAH," J. Acoust. Soc. Am. **78**(4), 1395–1413 (1985).
[8]W. A. Veronesi and J. D. Maynard, "Nearfield acoustic holography (NAH). II. Holographic reconstruction algorithms and computer implementation," J. Acoust. Soc. Am. **81**(5), 1307–1322 (1987).
[9]J. Pachner, "Investigation of scalar wave fields by means of instantaneous directivity patterns," J. Acoust. Soc. Am. **28**(1), 90–92 (1956).
[10]G. Weinreich and E. B. Arnold, "Method for measuring acoustic radiation fields," J. Acoust. Soc. Am. **68**(2), 404–411 (1980).
[11]X. Zhao and S. F. Wu, "Reconstruction of vibroacoustic fields in half-space by using hybrid near-field acoustical holography," J. Acoust. Soc. Am. **117**(2), 555–565 (2005).
[12]F. Jacobsen and V. Jaud, "Statistically optimized near field acoustic holography using an array of pressure-velocity probe," J. Acoust. Soc. Am. **121**(3), 1550–1558 (2007).
[13]Y.-B. Zhang, X.-Z. Chen, and F. Jacobsen, "A sound field separation technique based on measurements with pressure-velocity probes," J. Acoust. Soc. Am. **125**(6), 3518–3521 (2009).
[14]C. Langrenne, M. Melon, and A. Garcia, "Boundary element method for the acoustic characterization of a machine in bounded noisy environment," J. Acoust. Soc. Am. **121**(5), 2750–275 (2007).
[15]C.-X. Bi, X.-Z. Chen, and J. Chen, "Sound field separation technique based on equivalent source method and its application in nearfield acoustic holography," J. Acoust. Soc. Am. **123**(3), 1472–1478 (2008).
[16]J. Hald, "Time domain acoustical holography and its applications," Sound Vib. **35**, 16–24 (2001).
[17]J.-H. Thomas, V. Grulier, S. Paillasseur, J.-C. Pascal, and J.-C. Le Roux, "Real-time nearfield acoustical holography for continuously visualizing nonstationary acoustic fields," J. Acoust. Soc. Am. **128**(6), 3554–3567 (2010).
[18]S. Paillasseur, J.-H. Thomas, and J.-C. Pasca, "Regularization for improving the deconvolution in real-time near-field acoustic holography," J. Acoust. Soc. Am. **129**(6), 3777–3787 (2011).
[19]V. Grulier, S. Paillasseur, J.-H. Thomas, J.-C. Pascal, and J.-C. Le Roux, "Forward propagation of time evolving acoustic pressure: Formulation and investigation of the impulse response in time-wavenumber domain," J. Acoust. Soc. Am. **126**(5), 2367–2378 (2009).
[20]A. Tikhonov, "Solutions of incorrectly formulated problems and the regularization method," Sov. Math. Dokl. **4**, 1035–1038 (1963).
[21]P. C. Hansen and D. P. O'Leary, "The use of the L-curve in the regularization of discrete ill-posed problems," SIAM J. Sci. Comput. (USA) **14**, 1487–1503 (1993).